Article

Fabrication of Stable Cu-Ce Catalyst with Active Interfacial Sites for NOx Elimination by Flame Spray Pyrolysis

Xin Tong [1,2], Jiafeng Yu [1,*] , Ling Zhang [1,2] and Jian Sun [1,*]

1   Dalian Institute of Chemical Physics, Chinese Academy of Sciences, Dalian 116023, China;
     tongxin@dicp.ac.cn (X.T.); zhangling2020@dicp.ac.cn (L.Z.)
2   University of Chinese Academy of Sciences, Beijing 100049, China
*   Correspondence: yujf@dicp.ac.cn (J.Y.); sunj@dicp.ac.cn (J.S.)

Abstract: The complete conversion of NO_x to harmless N_2 without N_2O formation is crucial for the control of air pollution, especially at low temperatures. Cu-based catalysts are promising materials due to their low cost and high activity in NO dissociation, even comparable to noble metals; however, they suffer from low stability. Here, we established a Cu-Ce catalyst in one step with strong metal–support interaction by the flame spray pyrolysis (FSP) method. Almost 100% NO conversion was achieved at 100 °C, and they completely transferred into N_2 at a low temperature (200 °C) for the FSP-CuCe catalyst, exhibiting excellent performance in NO reduction by CO reaction. Moreover, the catalytic performance can stay stable, while 23% NO conversion was lost in the same condition for the one made by the co-precipitation (CP) method. This can be attributed to the synergistic effect of abundant active interfacial sites and more flexible surface oxygen created during the FSP process. The flame technology developed here provides an efficient way to fabricate strong metal–support interactions, exhibiting notable potential in the design of stable Cu-based catalysts.

Keywords: Cu-based catalysts; flame spray pyrolysis; NO_x elimination; active interfacial sites; high stability

1. Introduction

In recent years, air pollution has become serious and triggered a battle of survival for the ecosystem [1]. Nitrogen oxide (NO_x) is not only the source of nitric acid rain but is also one of the main substances forming chemical smog, becoming one of the most important air pollutants affecting human health [2]. With the large-scale extraction and consumption of fossil sources, nitrogen oxides emitted by combustion, industrial production processes and motor vehicles are inevitable [3]. NO_x is usually reduced by ammonia via the selective catalytic reduction (NH_3-SCR) process. However, its shortcomings such as the secondary pollution derived from NH_3 leakage and the destruction of air preheaters cannot be ignored [4]. In comparison, the catalytic reduction by CO molecules is supposed to be the ideal strategy given the present eco-friendly standards of the deNOx process, considering that the combustion of fossil energy often creates NO and CO molecules simultaneously. However, in this process, N_2 selectivity is hard to reach 100% due to the production of a large amount of by-product N_2O, especially at low temperatures [5,6]. Nowadays, N_2O is the third most important long-lived greenhouse gas after carbon dioxide and methane, as well as the most important agent in the depletion of the ozone layer [7]. Thus, the development of a highly efficient catalyst to reduce toxic NO into harmless N_2 without emission of N_2O is promising in the modern post-industrial society [8].

NO molecules must undergo dissociative chemisorption for their conversion to N_2, while CO should be molecularly adsorbed. Otherwise, molecularly adsorbed NO favors the formation of N_2O. Therefore, NO reduction by CO is a site-specific reaction with active sites for both CO adsorption and NO dissociation. Based on this, noble metals or Cu-supported

catalysts [9–11], Ce-based solid solution [12,13] and perovskites [14,15] have been rationally designed and systematically investigated. Noble metals have high catalytic activity for the complete reduction of NO into N_2, even at temperatures as low as 200–250 °C [10,16]. However, their scarcity, high price, and easy toxicity have greatly limited their applications. Given this, Cu-based catalysts represent a promising alternative from the viewpoint of low cost and similar efficiency. The NO conversion rate would reach 100% at around 230 °C on Mn-modified $CuFe_2O_4$ catalysts [17], and 90% of N_2 selectivity can be obtained at 200 °C on Cu/CeO_2-Fe_2O_3 catalysts [11]. Moreover, oxygen vacancies of oxide support exhibit a positive effect on the elimination of NO_x by prompt transfer of the active O derived from the dissociation of the N–O bond to avoid the formation of N_2O [18–20]. CeO_2 is widely used in NO_x emissions due to its high capability of oxygen storage and release through redox processes via Ce^{4+}/Ce^{3+} coupling [21–25], especially in improving low-temperature N_2 selectivity [26].

Based on the above analysis, the high activity of the CuO-CeO_2 catalyst is correlated with the synergism of copper–ceria interactions, with both components being significantly more readily reduced or oxidized than the corresponding independent ones. The interfacial sites between the CuO clusters and the CeO_2 support were more active relative to the individual phases due to their greater reducibility [27,28]. Synergetic effects in the CuO–CeO_2 catalysts have been generally recognized; however, the identification of different Cu species is difficult due to the existence of a variety of Cu species, such as finely dispersed CuO particles, Cu^{2+} with strong interaction with Ce or Cu^{2+} in the CeO_2 lattice, let alone the variations during the reaction. It has been reported that the efficiency of NO conversion is greatly affected by the Cu preparation method. For example, the deposition of CuO on perovskites by the precipitation or wet impregnation methods showed poor activity, allowing almost complete NO conversion only above 400 °C [29,30]. The co-precipitation method facilitated the formation of the incorporation of metals into CeO_2 for enhancing the movable oxygen, owing to the more sufficient contact among each component compared with the impregnation method. However, active metal species on the surface may also disappear. A more facile method that could create both surface-active sites and strong interactions is desirable. It has been demonstrated that flame spray pyrolysis (FSP) is a well-established single-step method to provide nano-sized supported catalysts [31,32]. It will not only efficiently disperse the active metals on the supports but also enhance the oxygen vacancies in Ce oxides lattice [33,34] and the metal–support interaction [35,36]. FSP can create lattice oxygen distortion and provide about 19 times more oxygen vacancies than traditional ones by quenching from an extremely high temperature [37], exhibiting great potential in accelerating NO_x reduction.

In this study, we systematically investigated the function of Cu-based catalysts in accelerating NO_x reduction without the help of any noble metals. With this work, we aim to design a new Cu-Ce composite oxide catalyst via the quenching process of FSP, creating both active Cu sites with strong metal–support interaction and Cu dopants in CeO_2 lattice in one-step synthesis. The Cu species are active in NO dissociation and CO adsorption, while the distortion structure in CeO_2 will create abundant oxygen vacancies, facilitating O removal and N_2 production at low temperatures. Moreover, the strong Cu-Ce interaction formed at high temperatures during the preparation process will inhibit metal sintering and enhance the stability of catalysts. NO reduction by CO was chosen as a probe reaction to evaluate their catalytic performance, focusing on the reaction rate of NO and the selectivity of N_2 at low temperatures. The structures of the synthesized catalysts and the reaction mechanism are discussed following the characterizations. The results will pave the way for the rational design of Cu-based catalysts with extremely high activity at low temperatures and anti-sintering properties for applications.

2. Results and Discussion

2.1. Catalytic Performances

NO, as one of the main pollutants in the emission, is expected to be selectively reduced to N_2 instead of the by-product N_2O. The catalytic property of Cu-Ce oxide catalysts with different Cu contents (1 wt % and 10 wt %) synthesized by FSP and CP for NO reduction was explored at 100–400 °C, as observed in Figure 1a–c. NO conversion, CO conversion and N_2 selectivity increased with reaction temperature for all of the tested catalysts, but they exhibited distinguished activity at low temperatures. For the CeO_2 sample, the NO cannot be completely activated and reduced until 450 °C due to the absence of active metals, although the consumed NO can be converted into N_2 at 350 °C with the assistance of oxygen vacancies in CeO_2 lattice. When adding a small amount of Cu (1 wt %), the NO reduction activity was improved, and the 100% conversion temperature was decreased to 220 °C. It further decreased to a temperature as low as 175 °C with increasing Cu content to 10 wt %. The light-off temperature (T_{50}) dropped down to almost 160 °C and 180 °C after adding 1 wt % and 10 wt % Cu in CeO_2 via the FSP method, respectively. The FSP-CuCe with high Cu content (10%) exhibited the best activity, especially for N_2 selectivity, while those synthesized by the CP method were completely different. The performance of CP-CuCe with low Cu content was more active than the one with high Cu content at low temperature, but the order was reversed above 200 °C, because the complete conversion of NO and CO cannot be obtained until 400 °C for the former. Although the NO was fully eliminated at about 200 °C over the CP-CuCe(10) sample, it can only be partially reduced into N_2O, resulting in the N_2 selectivity being below 5% at the same temperature. As shown in Figure 1d, the activity of FSP-CeCu(10) can be further improved in the mixture of 2% CO and 1% NO atmosphere, where NO conversion can reach 100% at 100 °C. Afterward, N_2 selectivity gradually increased until 200 °C, indicating that N_2O can be completely suppressed at such a low temperature. The catalytic performance of FSP-CuCe(10) has advantages in the reported Cu-based catalysts for the NO + CO reaction. For example, a Cu-Ni catalyst completely converted NO to N_2 at above 350 °C [38]. The temperature was decreased to 275 °C over Cu-Mn [39] and 250 °C over Cu-Ce [40] catalysts. The catalyst was further optimized by using CeO_2-Fe_2O_3 as the support, and 90% NO conversion was achieved at 200 °C [11]. The activity of FSP-CuCe(10) was comparable to the 1%Pd/Fe-CeO_2 catalyst recently reported [26], indicating that the FSP-made CuCe catalyst in this work exhibits potential in the substitution of noble metal utilization in the elimination of NO_x (NO and N_2O) pollutants in an extremely low temperature range.

Generally, Cu-based catalyst was famous for its high activity but suffered from poor stability. During the stability test at different conditions in Figure 2a, the CP-CuCe(10) catalyst was severely deactivated, with the NO conversion decreased from 100% to 77% in 40 h, while the catalytic performance of FSP-CuCe(10) kept constant even in the condition of high GHSV. Meanwhile, the N_2 selectivity slightly increased from 85% to 92%, which was much higher than that of the CP-CuCe(10) catalyst. This indicated that the amount of Cu active sites for NO dissociation decreased probably due to the aggregation of Cu particles. Usually, the CuCe catalysts were active without reduction before NO + CO reaction. For fresh FSP-CuCe(10), the activity was high without any pretreatment in the first-round test. Interestingly, NO conversion in the second-round test was enhanced compared to the first one, as shown in Figure 2b, indicating that special Cu species were formed and can be activated in the reaction conditions. On the contrary, slight deactivation was observed over the CP-CuCe catalyst.
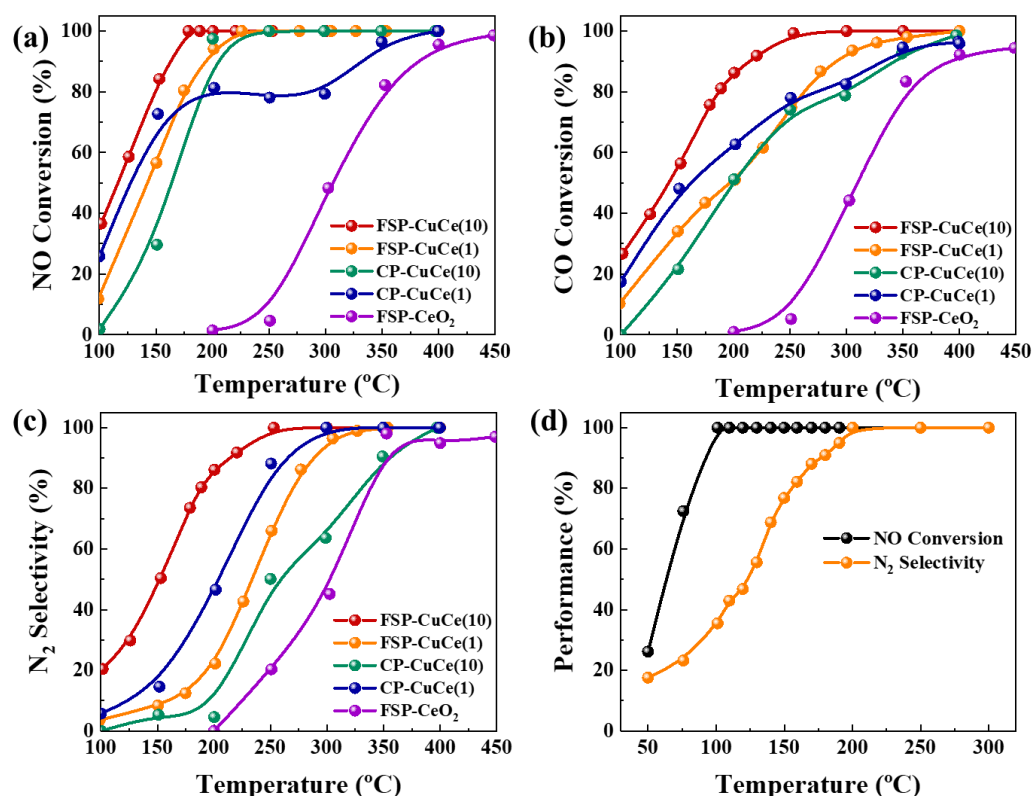
Figure 1. Comparison of catalytic performance of CuCe catalysts synthesized by FSP and CP methods with Cu weight percentage of 1% and 10% over NO + CO reaction (5%NO + 5%CO + 90%He): (**a**) NO conversion, (**b**) CO conversion and (**c**) N_2 selectivity. (**d**) The performance of FSP-CuCe(10) sample in 1%NO + 2%CO + 97%He reaction atmosphere.
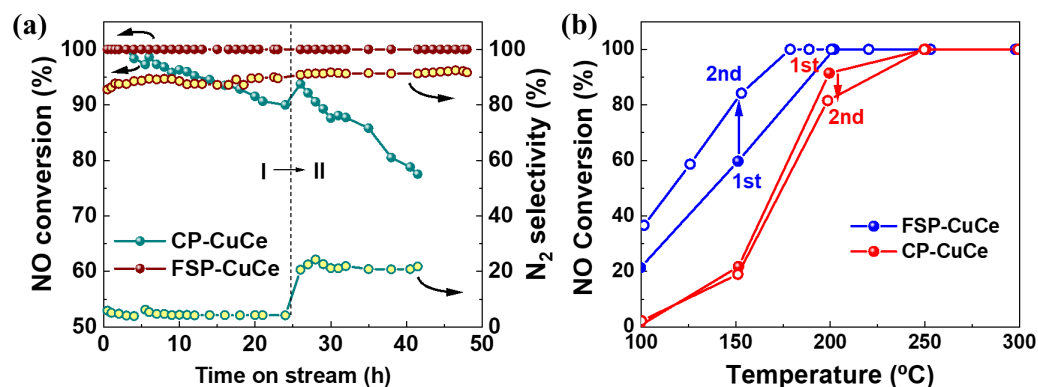

Figure 2. Stability test of typical catalysts: (**a**) The stability of FSP-CuCe and CP-CuCe catalysts at different conditions (I: 200 °C with GHSV = 15,000 mL/(g·h) and II: 250 °C with GHSV = 60,000 mL/(g·h); (**b**) NO reduction performance of FSP-CuCe and CP-CuCe catalysts in two test cycles (first is solid and second is hollow) in NO + CO reaction.

2.2. Crystal Structure and Morphology Analysis

The X-ray diffraction patterns of fresh and used samples are shown in Figure 3, where six peaks were observed in all the patterns for 2θ varying from 20° to 80°. These peaks can be assigned to (111), (200), (220), (311), (222) and (400) planes of the typical face-centered cubic fluorite structure of CeO_2. The peak width at half height of FSP-made samples was narrower than that of CP-made ones, which implies that the particle size increased when they were produced from high-temperature flames in the FSP process according to the Scherrer equation. The growth of $FSP-CeO_2$ particles during the reaction was also observed,

while the one with Cu was stable. Two peaks related to the CuO phase (PDF: 01-080-1917) were found on the fresh FSP-CuCe sample, while no extra peaks assigned to the Cu or Cu_2O phase were observed in the patterns of the used FSP-CuCe sample, which may be explained by the fact that the Cu nanoparticles were re-dispersed during the reaction and too small to be detected by XRD. Moreover, from the magnification of the (111) plane, the peak position was the same with standard CeO_2 for FSP-CuCe and CP-CuCe samples; however, the shift to a high degree during the reaction can only be detected for the FSP-made sample. Thus, it could be deduced that copper cations were embedded into CeO_2 lattice due to the intimate contact of Cu and Ce ions in the solution and the high temperature of the flame in the process of FSP preparation, which has been reported before [41–43]. The incorporation was further enhanced in the reduced atmosphere during the reaction accompanied by lattice shrink, since the radius of Cu^{2+} ions (0.072 nm) is smaller than that of Ce^{4+} (0.097 nm) [44]. The morphology of the samples was revealed by scanning electron microscopy (SEM) and transmission electron microscopy (TEM), as shown in Figure 4. From SEM images, the FSP-CuCe catalyst was small and had uniform nanosized particles, while there were various sizes of particles in the CP-CuCe sample, composed of small crystallites with irregular shapes and large particles with sizes of a few micrometers. From TEM images, the shape of the FSP-CuCe nanoparticles was cubic with distinct lattice fringes, while those in the CP-CuCe sample were sphere-like nanostructures.
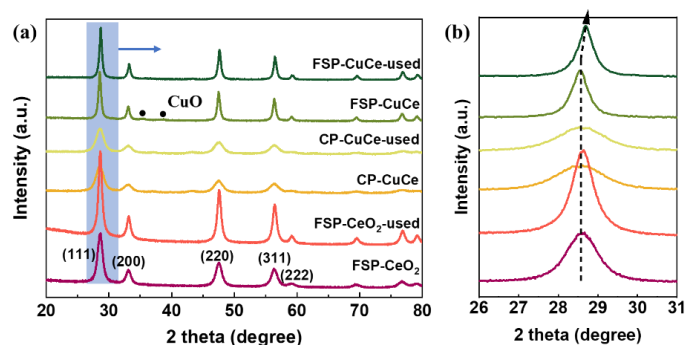

Figure 3. Lattice structure evaluation: (**a**) XRD patterns of fresh and used samples, including FSP-CeO_2, FSP-CuCe(10) and CP-CuCe(10) catalysts; (**b**) the magnification of marked area.
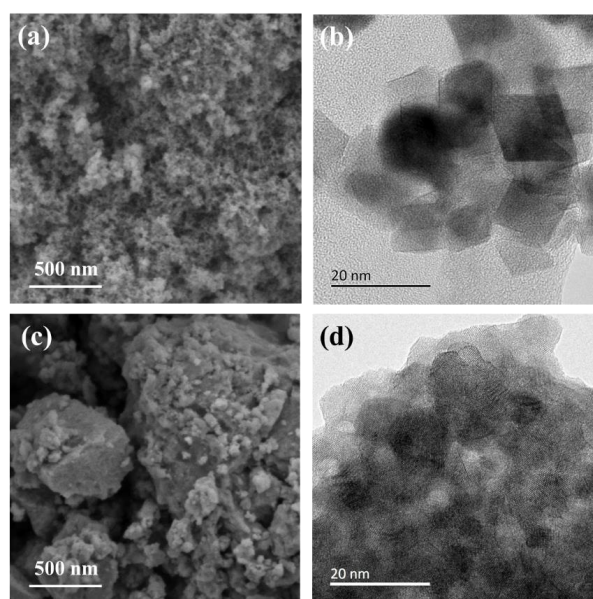

Figure 4. Morphology of materials: SEM (**a**,**c**) and TEM (**b**,**d**) micrographs of FSP-CuCe(10) (**a**,**b**) and CP-CuCe(10) (**c**,**d**) catalysts.

2.3. Oxygen Species Analysis

2.3.1. Raman

Further insight into the incorporation of Cu ions into the CeO_2 lattice can be achieved by Raman spectroscopy. In Figure 5, the strong peak that appeared at around 463 cm^{-1} for all tested catalysts can be assigned to the F_{2g} mode of the cubic fluorite CeO_2 structure. The downshift of the F_{2g} Raman peak is known to be related to the concentration of oxygen vacancy. The redshift of the F_{2g} mode band for the CP-CuCe sample from 463 to 451 cm^{-1} was larger than that of FSP-CuCe from 463 to 458 cm^{-1}, indicating that the amount of Cu incorporation in the CeO_2 lattice, accompanied by the generation of oxygen vacancies for charge balance [45], was greater for the former than the latter. Moreover, the bands at 223 and 570 cm^{-1}, which are also ascribed to the evolution of oxygen vacancies, showed the same trend. After reduction at 200 °C by CO, the F_{2g} mode band of FSP-CuCe further shifted to 453 cm^{-1} and then turned back to 458 cm^{-1} after reaction, while changes were observed in the same process for CP-CuCe. This demonstrated that the surface oxygen was easier reduced and oxidized in the different atmospheres for FSP-CuCe, exhibiting higher redox capability in the aspect of mobile oxygen. It appears that the CP-CuCe catalyst could create more surface oxygen vacancies than FSP-CuCe in the fresh sample state; however, more oxygen vacancies will be formed in the reduction or reaction atmosphere for the latter, as discovered in the following sections.
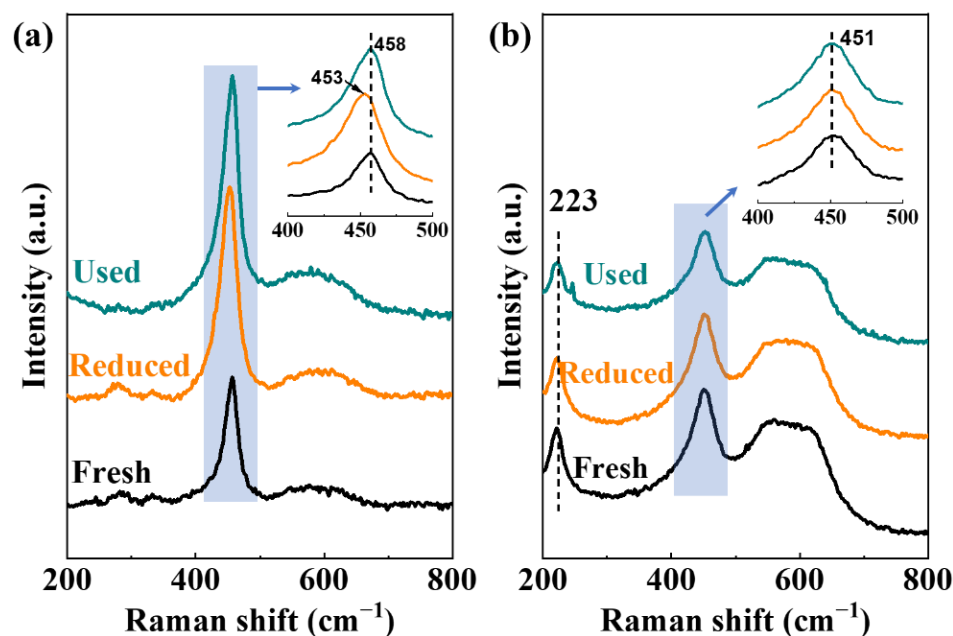

Figure 5. Raman spectra of fresh, reduced and used (**a**) FSP-CuCe and (**b**) CP-CuCe catalysts. The magnification of CeO_2 F_{2g} peak is shown as inserts.

2.3.2. CO-TPR

The reduction behavior of the catalysts was studied by CO-TPR technique since CO was the only reductant in the reaction. From Figure 6a, the reduction of bulk CeO_2 does not occur until 800 °C, while the mixture of CuO and CeO_2 powders exhibits two reduction peaks at low temperatures. The peak at 142 °C can be assigned to the reduction of small clusters on the surface CuO particles, and the one at 167 °C was derived from the bulk CuO phase. In comparison, only one symmetrical peak can be observed for the FSP-CuCe catalyst at 190 °C, which was much higher than that for CuO, implying that a strong interaction was formed between highly dispersed copper oxide and ceria. Moreover, this interaction can be further enhanced during the reaction, given that the reduction temperature of the used FSP-CuCe sample was increased to 230 °C. On the contrary, for CP-CuCe, the reduction

process occurred at about 300 °C and lasted to 800 °C without any observation of Cu species at low temperatures. The enhanced reducibility of lattice oxygen in CeO_2 was probably attributed to the incorporation of Cu and the generation of lattice distortion.
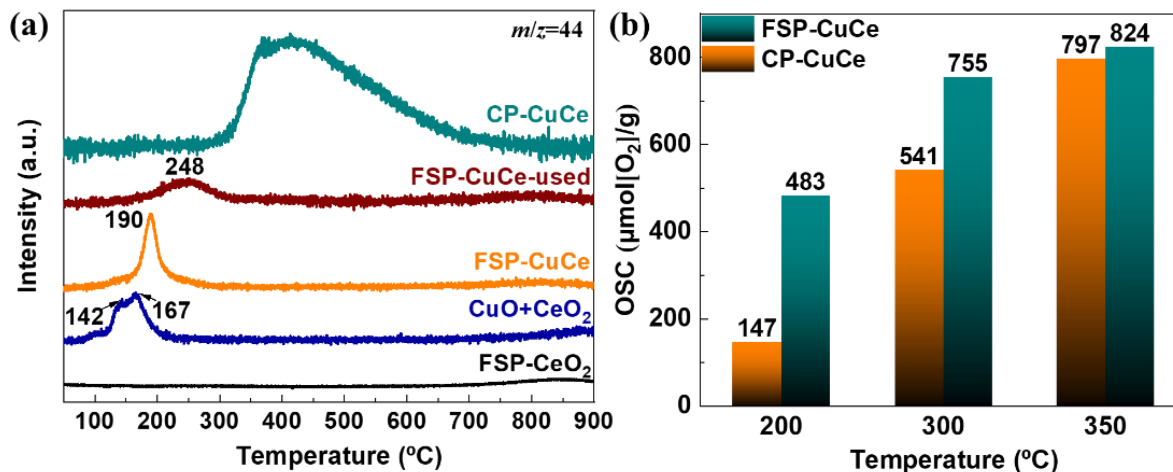

Figure 6. Reduction behavior of Cu and Ce species. (**a**) CO_2 generation ($m/z = 44$) profiles during CO-TPR of $FSP-CeO_2$, the physical mixture of CuO and CeO_2 powders (CuO + CeO_2), FSP-CuCe, used FSP-CuCe and CP-CuCe. (**b**) Oxygen storage capability (OSC) values for FSP-CuCe and CP-CuCe catalysts evaluated at different temperatures.

2.3.3. Oxygen Storage Capacity

The oxygen storage capacity (OSC) of samples is regarded as one of the most important parameters to evaluate mobile oxygen [46,47]. After oxidation pretreatment by $5\%O_2/He$, a CO pulse was conducted and the CO_2 generation signal was monitored by mass spectroscopy at three different temperatures, as illustrated in Figure 6b. The OSC was enhanced by increasing the operating temperature from 483 to 824 μmol/g for the FSP-CuCe catalyst, which was higher than that of CP-CuCe, especially at low temperatures. The mobile oxygen played an important role in NO reduction activity, which might be the reason that FSP-CuCe could reach 90% N_2 selectivity, while it was only 5% for CP-CuCe sample in the same conditions. Much higher OSC at low temperatures was attributed to the strong interaction between highly dispersed copper oxide and ceria, which could play a significant role in catalytic activity [48].

2.3.4. NO Pulse

Generally, NO reduction by CO is a two-step reaction: $CO + 2NO \rightarrow N_2O + CO_2$ and $CO + N_2O \rightarrow N_2 + CO_2$ [49], where N_2O is the main by-product of incomplete NO reduction, especially at low temperatures (below 300 °C) [50]. Therefore, it is essential to control the generation of active O from NO dissociation and the reduction of lattice oxygen by CO, requiring a high regeneration rate of oxygen vacancies to promptly remove active O. NO pulse chemisorption was conducted to evaluate the rate of NO dissociation and oxygen transfer by monitoring the products, as shown in Figure 7a,b. N_2 and N_2O were the main products when introducing NO for all tested samples. Total consumption of NO for FSP-CuCe and CP-CuCe were 320 and 259 μmol[NO]/g, respectively. From the residue NO signal, it can be found that the FSP-CuCe sample could convert more NO in one pulse at the beginning with N_2 as the main product due to the abundant oxygen vacancies. Then, the rate of NO consumption decreased to a low level and kept constant according to the observation of products in the last pulse. It is worth noting that the generation of by-product N_2O was low in all pulses, revealing that the rate of NO dissociation decreased with the decrement in oxygen vacancies. On the contrary, the signal of N_2 decreased and N_2O became the main product with oxygen vacancies consumption in the CP-CuCe

sample. The NO dissociation rate was still high with the lack of oxygen vacancies, leading to a large amount of N_2O emission instead of N_2. This implied that the appropriate NO dissociation and quick oxygen vacancies generation were essential for the redox cycle, preventing the recombination of redundant active O and N into N_2O. To further investigate the reduction behavior of N_2O, N_2O pulse chemisorption was also conducted at 200 °C, as shown in Figure 7c,d. The rate of N_2O reduction into N_2 was quicker on FSP-CuCe than on CP-CuCe. The total consumption of N_2O was 160 and 95 μmol[N_2O]/g for FSP and CP catalysts, respectively, demonstrating that the former was more active in both NO and N_2O conversion than the latter.

Figure 7. Monitoring of NO consumption and product formation during NO pulses by the mass spectrometer at 200 °C over (**a**) FSP-CuCe and (**b**) CP-CuCe catalysts. Monitoring of N_2O consumption and N_2 formation during N_2O pulses by the mass spectrometer at 200 °C over (**c**) FSP-CuCe and (**d**) CP-CuCe catalysts. The samples were firstly reduced by CO at 200 °C, then 5%NO/He or 5%N_2O/He was pulsed into the reactor.

2.4. Surface Species Identification

2.4.1. N$_2$O Pulse Chemisorption

N$_2$O is usually used for the measurement of exposed metallic Cu active sites on the surface of catalysts due to the partial oxidation of Cu^0 to Cu$^+$ species by the reaction of Cu + N$_2$O → Cu$_2$O + N$_2$ at low temperature. Therefore, the N$_2$O pulse chemisorption was also conducted at 50 °C to evaluate the active Cu sites on the surface. As shown in Figure 8, N$_2$O was obviously converted into N$_2$ for FSP-CuCe, while no clear reduction of the N$_2$O signal can be detected for the CP-CuCe sample even in the first pulse. The total N$_2$O consumption for them was 109 and 2μmol[N$_2$O]/g, respectively. This revealed that there were no metallic Cu species on the surface of CP-CuCe after CO reduction at 200 °C, leading to the lack of active sites for NO and CO activation. This result was consistent with CO-TPR, where the reduction of Cu species was undetectable.
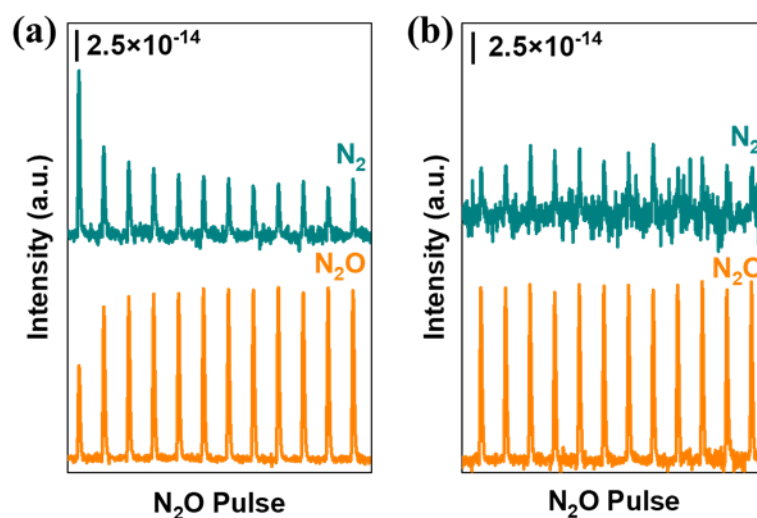

Figure 8. Monitoring of N$_2$O consumption and N$_2$ formation during N$_2$O pulses by mass spectrometer at 50 °C over (**a**) FSP-CuCe and (**b**) CP-CuCe catalysts. The samples were firstly reduced by CO at 200 °C, then 5%N$_2$O/He was pulsed into the reactor 12 times.

2.4.2. XPS

XPS was conducted to study the chemical state of the elements and oxygen species via Ce 3d and O 1s spectra. As shown from Ce 3d spectra in Figure 9a, six peaks (*v*, *v″* and *v‴* of Ce 3$d_{5/2}$ as well as *u*, *u″* and *u‴* of Ce 3$d_{3/2}$) can be assigned to Ce^{4+} species, while *v′* and *u′* features (marked with orange) belonged to Ce^{3+} species [51]. The reduction degree of ceria can be estimated by the Ce^{3+} content in total Ce [52]. The XPS spectra in the O 1s region can be deconvoluted into two peaks, as shown in Figure 9b. The main peak O$_\alpha$ at 529.1–529.4 eV is assigned to the characteristic lattice oxygen bonding to the metal cations (dyed in green), while O$_\beta$ with higher binding energy at 531.1–531.4 eV represented the surface chemisorbed oxygen such as O^{2-}, O$^-$ or adsorbed oxygen species from hydroxyl or water species on the surface (dyed in orange) [53,54]. From the summary of the fitting results in Figure 9c, the percentages of reduced cerium ions (Ce^{3+}) for the studied samples were more or less the same for both FSP- and CP-made CuCe samples, and they can remain stable during redox cycles in reaction. Although the Cu species were different produced by FSP and CP methods, the enhancement of surface Ce^{3+} species was similar, indicating that the Cu particles on the surface could also create Ce^{3+} species through the metal–support interface. It has been reported that the formation of surface chemisorbed oxygen O$_\beta$ was essential for redox reactions by enhancing oxygen mobility of the catalysts [55]. The active O$_\beta$ species can remain stable during reaction in the CP-CuCe catalyst, while they were greatly enhanced from 18.5% to 39.3% during reaction for FSP-CuCe. Therefore, it

is expected that the enhanced oxygen mobility of the FSP-CuCe catalyst results in high activity for NO + CO reaction, especially in the second-round test.
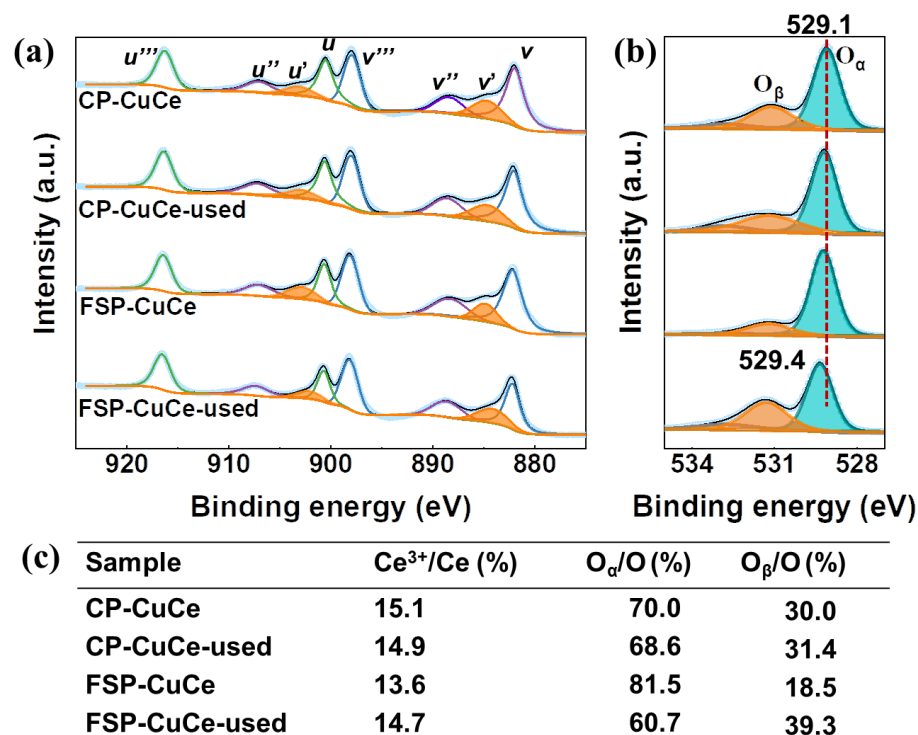

Figure 9. XPS spectra of (**a**) Ce 3*d* and (**b**) O 1*s* over FSP-CuCe and CP-CuCe, as well as their used samples. (**c**) Summary of surface compositions of Ce^{3+} and different oxygen species derived from XPS spectra.

The XPS spectra of Cu 2*p* are presented in Figure 10a for the fresh and used FSP-CuCe samples, as well as the used one with Ar^+ ion etching treatment to eliminate the effect of oxidation in the air on the valence state of Cu species. Usually, Cu^{2+} has an observable collection of satellite features between 939.0 and 945.8 eV. The presence of reduced Cu species can be estimated by the ratio between the intensity of the shake-up satellite peak and the main Cu $2p_{3/2}$ peak (0.55) [56]. For all measured samples, the peaks for Cu $2p_{3/2}$ (933.7 eV) were much larger than the satellite peaks, indicating that they contained both Cu^{2+} and reduced Cu species (Cu^0 and Cu^+). The fitting for Cu 2*p* was performed following the split spin–orbit rules with a distance of 19.75 eV and an intensity ratio of 0.508. The one that belonged to Cu^{2+} was marked as orange with a center at about 933.5 eV, while the reduced Cu species were in blue at about 932.5 eV. The distinction of Cu^0 and Cu^+ species was further performed by Cu *LMM* Auger peaks at 918.6 and 916.8 eV (Figure 10b). The content of different Cu species is summarized in Figure 10c. Almost half of Cu species were in a +2 oxidation state accompanied by 30% Cu^+ in the fresh FSP-CuCe sample. Moreover, a significant reduction of Cu^{2+} to Cu^+ was observed during the reaction since the Cu^+ was increased to 43.1% after the reaction. From the comparison to the etched sample, Cu^+ species were stable even when exposed to the air, while Cu^0 was more readily oxidized to CuO. It was reported that the existence of Cu^+ can be attributed to its bigger electronegativity due to the shift of electron conversion redox equilibrium from Ce^{3+} to Cu^+ [57]. Then, the formation of low-valent state Cu species can effectively promote the reduction of Ce^{4+} species to Ce^{3+} species. This redox process of Ce^{4+}/Ce^{3+} at the interfacial position could also be connected with the formation of the defect structure with oxygen vacancies, resulting in the enhancement of oxygen mobility.
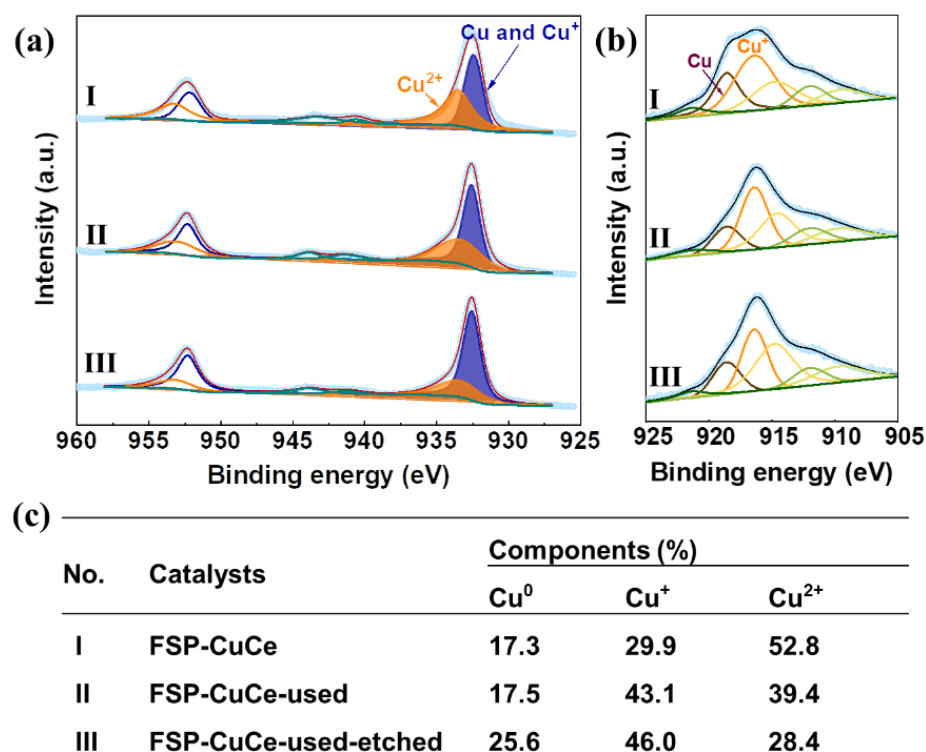
Figure 10. (**a**) XPS spectra of Cu 2*p* and (**b**) Auger electron spectroscopy (AES) of Cu *LMM* over fresh and used FSP-CuCe, as well as the used one with etching treatment. (**c**) Summary of surface compositions of different Cu species derived from XPS spectra.

Based on the above analysis, the reaction mechanism was proposed for NO reduction by CO over the FSP-CuCe catalyst. On one hand, the mobility of oxygen was enhanced due to the active interfacial created by the strong interaction between Cu particles and the CeO_2 support by the redox equilibrium between Ce^{3+} and Cu^+, resulting in the promotion of active O removal and the suppression of by-product N_2O formation. This strong interaction was attributed to the FSP method, where small liquid droplets were firstly produced by a high-speed gas flow and then decomposed into nanoparticles via combustion at extremely high temperatures (about 2000 °C) [58]. The following rapid quenching with the help of high-speed flowing air and cooling water [59] was used to inhibit particle growth due to sintering. The direct production of catalyst powder in one step without further calcination would benefit the distortion structure. On the other hand, the metallic Cu formed during the FSP method was an active site of NO dissociation and CO activation, which also facilitated the conversion of NO at low temperatures. It has been reported that the finely dispersed species possessed the highest activity, better than the bulk CuO, while the Cu^{2+} in the CeO_2 lattice was the lowest [60]. Therefore, although the doping of Cu in the CeO_2 lattice facilitated the oxygen storage capacity, the synergistic effect of Cu active sites and the mobile oxygen on the surface was essential for the excellent catalytic performance of the FSP-CuCe catalyst.

3. Materials and Methods

3.1. Materials Preparation

Flame spray pyrolysis (FSP) method. The FSP samples were prepared by using the homemade set-up reported in our previous work [38]. Appropriate amounts of cerium (III) 2-ethylhexanoate (49% in 2-ethylhexanoic acid, 12% Ce) and copper (II) acetate were dissolved in a mixture of xylene and 2-ethylhexanoic acid (volume ratio = 1:1). The total concentration of Ce + Cu in the liquid precursor was set at 0.5 M. The precursor was fed to the flame using a syringe pump (TYD02, LEAD FLUID) with a rate of 5 mL/min and

dispersed by oxygen (feed rate 3.5 L/min and pressure 1.5 bar). The flame was ignited by premixed methane (0.6 L/min) and oxygen (1.9 L/min) issued from an annular gap. The product particles were blown up with the assistance of a vacuum pump and collected by a water-cooled glass fiber filter (Whatman GF 6, 240 mm in diameter) on the top. The catalysts with different Cu contents (1 wt % and 10 wt %) are denoted as FSP-CuCe(1) and FSP-CuCe(10). The FSP-CuCe(10) sample is simplified as FSP-CuCe in the characterizations.

Co-precipitation (CP) method. Adequate amounts of cerium (III) nitrate and copper (II) nitrate were dissolved in deionized water to a total cation concentration of 0.3 mol/L. Then, the $(NH_4)_2CO_3$ solution (1 mol/L) was slowly added to the above solution at 50 °C with continuous stirring until the pH value reached 10. The suspensions were aged for another 2 h at 50 °C. Then, the solution was centrifuged at room temperature and washed until pH = 7.0. The obtained precipitate was dried at 110 °C for 12 h and calcined in air at 500 °C for 4 h. The catalysts with different Cu contents (1 wt % and 10 wt %) are denoted as CP-CuCe(1) and CP-CuCe(10). The CP-CuCe(10) sample is simplified as CP-CuCe in the characterizations.

3.2. Catalytic Performance

Catalytic activity test. Catalytic tests were carried out with a fixed-bed quartz reactor, where 100 mg catalyst was held in the middle. Mixtures of NO, CO and He with different concentrations (5 vol % NO, 5 vol % CO and 90 vol % He, as well as 1 vol % NO, 2 vol % CO and 97 vol % He) were fed to the reactor at a flow rate of 25 mL/min. The outlet gas was separated by a Porapak Q packed column with a heating program and analyzed by an online GC with a TCD detector.

3.3. Characterizations

Powder X-ray diffraction (XRD) patterns were recorded on an X'Pert Pro (PANalytical XRD, X'Pert Pro MPD, Almelo, the Netherlands) diffractometer with Cu Kα radiation at 40 kV and 40 mA over a 2θ range from 5° to 80°. The surface morphology of catalysts was characterized by scanning electron microscopy (SEM, JSM-7800F, JEOL, Tokyo, Japan). Transmission electron microscopy (TEM) was carried out with a JEM 2100 microscope with an accelerating voltage of 200 kV. Raman spectra were collected on a Renishaw inVia Laser Raman spectrometer using an Ar$^+$ laser beam. The Raman spectra were recorded using a Bruker Optics Raman spectrometer with a laser excitation energy of 532 nm and a laser power of 2 mW. The oxygen storage capacity (OSC) was measured by the BELCAT II Chemisorption analyzer. Then, 10 mg catalysts were pretreated in 5%O_2/He for 30 min and 996 μL 5%CO/He was pulsed into the reactor 12 times at different temperatures (200, 300 and 350 °C) via monitoring the CO and produced a CO_2 signal (m/z = 28 and 44, respectively) from a Pfeiffer OmniStar mass spectrum. The amount of CO consumed during all the pulse experiments is referred to as the total OSC. X-ray photoelectron spectroscopy (XPS) was tested on a Thermo ESCALAB 250XI equipment with Al Kα X-ray source (hv = 1486.6 eV and passing energy of 30 eV). Adventitious C 1s (284.8 eV) was used to compensate for the surface charge effects. NO pulse and N_2O pulse experiments were performed on the same chemisorption analyzer. Firstly, 20 mg of the sample was pretreated in CO at 200 °C for 30 min. Then, 5%NO/He was pulsed into the reactor 12 times (996 μL per pulse) at the same temperature. For the N_2O pulse experiment, 5%N_2O/He was pulsed into the reactor 12 times (996 μL per pulse) at both 50 °C and 200 °C. The N_2, N_2O and NO signals (m/z = 28, 44 and 30, respectively) were recorded by a mass spectrometer.

4. Conclusions

We established a Cu-Ce catalyst with strong metal–support interaction between highly dispersed copper oxide and ceria in one step by the FSP method. NO conversion reached 100% at as low as 100 °C; then, the formation of by-product N_2O was effectively suppressed with increasing temperature and undetectable at 200 °C. Moreover, high stability of the

FSP-Cu-Ce catalyst without any detection of deactivation was achieved, while NO conversion decreased from 100% to 77% in the same condition for the catalyst made by the CP method. Characterizations revealed that surface Cu oxides could be partially reduced and incorporated into CeO_2 lattice at the interface of FSP-CuCe during the reaction, strengthening the synergistic effect of N−O bond activation and oxygen transfer. NO dissociation and the subsequent oxygen transfer through oxygen vacancies were remarkably accelerated at low temperatures due to the formation of active interfacial sites. The flame technology is thus demonstrated to be an efficient way to fabricate active and stable Cu-based catalysts, which is promising in the reduction or substitution of noble metals in NO_x elimination.

Author Contributions: X.T.: Investigation, data curation; J.Y.: Supervision, conceptualization, formal analysis, writing, funding acquisition; L.Z.: Investigation, data curation; J.S.: Supervision, funding acquisition. All authors have read and agreed to the published version of the manuscript.

Data Availability Statement: All relevant data are available from the corresponding author on request.

Conflicts of Interest: The authors declare no conflict of interest.

References

1. Agathokleous, E.; Sicard, P. Editorial Overview: Current and Future Challenges of Air Pollution. *Curr. Opin. Environ. Sci. Health* **2021**, *21*, 100246. [CrossRef]
2. De Vries, W. Impacts of Nitrogen Emissions on Ecosystems and Human Health: A Mini Review. *Curr. Opin. Environ. Sci. Health* **2021**, *21*, 100249. [CrossRef]
3. Khivantsev, K.; Vargas, C.G.; Tian, J.; Kovarik, L.; Jaegers, N.R.; Szanyi, J.; Wang, Y. Economizing on Precious Metals in Three-Way Catalysts: Thermally Stable and Highly Active Single-Atom Rhodium on Ceria for NO Abatement under Dry and Industrially Relevant Conditions. *Angew. Chem. Int. Ed.* **2021**, *60*, 391–398. [CrossRef] [PubMed]
4. Cheng, X.; Xiao, X.; Yin, Y.; Wang, J.; Qiao, W.; Ling, L. Ammonia-Free Selective Catalytic Reduction of NO at Low Temperature on Melamine Impregnated MnO_x–CeO_2/Carbon Aerogels. *Ind. Eng. Chem. Res.* **2021**, *60*, 13233–13242. [CrossRef]
5. Roy, S.; Marimuthu, A.; Hegde, M.; Madras, G. High Rates of NO and N2O Reduction by CO, CO and Hydrocarbon Oxidation by O_2 over Nano Crystalline Ce0.98Pd0.02O2−δ: Catalytic and Kinetic Studies. *Appl. Catal. B Environ.* **2007**, *71*, 23–31. [CrossRef]
6. Takigawa, A.; Matsunami, A.; Arai, N.; Peng, Y.Z. Effects of CO and H_2 on the Formation of N_2O via Catalytic NO Reduction. *Energy* **2005**, *30*, 475–484. [CrossRef]
7. Ravishankara, A.R.; John, S.D.; Robert, W.P. Nitrous Oxide (N_2O): The Dominant Ozone-Depleting Substance Emitted in the 21st Century. *Science* **2009**, *326*, 123–125. [CrossRef]
8. Roy, S.; Hegde, M.; Madras, G. Catalysis for NOx Abatement. *Appl. Energy* **2009**, *86*, 2283–2297. [CrossRef]
9. Ueda, K.; Tsuji, M.; Ohyama, J.; Satsuma, A. Tandem Base-Metal Oxide Catalyst: Superior NO Reduction Performance to the Rh Catalyst in NO–C_3H_6–CO–O_2. *ACS Catal.* **2019**, *9*, 2866–2869. [CrossRef]
10. Hu, Q.; Cao, K.; Lang, Y.; Chen, R.; Chu, S.; Jia, L.; Yue, J.; Shan, B. Improved NO–CO Reactivity of Highly Dispersed Pt Particles on CeO2 Nanorod Catalysts Prepared by Atomic Layer Deposition. *Catal. Sci. Technol.* **2019**, *9*, 2664–2672. [CrossRef]
11. Cheng, X.; Zhang, X.; Su, D.; Wang, Z.; Chang, J.; Ma, C. NO Reduction by CO over Copper Catalyst Supported on Mixed CeO_2 and Fe_2O_3: Catalyst Design and Activity Test. *Appl. Catal. B Environ.* **2018**, *239*, 485–501. [CrossRef]
12. Wang, Q.; Li, G.; Zhao, B.; Shen, M.; Zhou, R. The Effect of La Doping on the Structure of Ce0.2Zr0.8O2 and the Catalytic Per-Formance of Its Supported Pd-Only Three-Way Catalyst. *Appl. Catal. B Environ.* **2010**, *101*, 150–159. [CrossRef]
13. Yao, X.; Xiong, Y.; Zou, W.; Zhang, L.; Wu, S.; Dong, X.; Gao, F.; Deng, Y.; Tang, C.; Chen, Z.; et al. Correlation Between the Physicochemical Properties and Catalytic Performances of CexSn1–xO2 Mixed Oxides for NO Reduction by CO. *Appl. Catal. B Environ.* **2014**, *144*, 152–165. [CrossRef]
14. Wu, Y.; Li, D.; Lu, J.; Xie, S.; Dong, L.; Fan, M.; Li, B. LaMnO3-La2CuO4 Two-Phase Synergistic System with Broad Active Window in NOx Efficient Reduction. *Mol. Catal.* **2020**, *493*, 111111. [CrossRef]
15. Schön, A.; Dacquin, J.-P.; Granger, P.; Dujardin, C. Non Stoichiometric La1-YFeO$_3$ Perovskite-Based Catalysts As Alternative to Commercial Three-Way-Catalysts?—Impact of Cu and Rh Doping. *Appl. Catal. B Environ.* **2018**, *223*, 167–176. [CrossRef]
16. Guo, S.; Zhang, G.; Han, Z.-K.; Zhang, S.; Sarker, D.; Xu, W.W.; Pan, X.; Li, G.; Baiker, A. Synergistic Effects of Ternary PdO–CeO2–OMS-2 Catalyst Afford High Catalytic Performance and Stability in the Reduction of NO With CO. *ACS Appl. Mater. Interfaces* **2021**, *13*, 622–630. [CrossRef] [PubMed]

17. Shi, X.; Chu, B.; Wang, F.; Wei, X.; Teng, L.; Fan, M.; Li, B.; Dong, L.; Dong, L. Mn-Modified CuO, $CuFe_2O_4$, and γ-Fe_2O_3 Three-Phase Strong Synergistic Coexistence Catalyst System for NO Reduction by CO With a Wider Active Window. *ACS Appl. Mater. Interfaces* **2018**, *10*, 40509–40522. [CrossRef]

18. Carollo, G.; Garbujo, A.; Xin, Q.; Fabro, J.; Cool, P.; Canu, P.; Glisenti, A. $CuO/La_{0.5}Sr_{0.5}CoO_3$ Nanocomposites in TWC. *Appl. Catal. B Environ.* **2019**, *255*, 117753. [CrossRef]

19. Hong, W.-J.; Ueda, M.; Iwamoto, S.; Hosokawa, S.; Wada, K.; Kanai, H.; Deguchi, H.; Inoue, M. Effect of Fe Content on Physical Properties of BaO–$CeOx$–$FeOy$ Catalysts for Direct NO Decomposition. *Appl. Catal. B Environ.* **2011**, *106*, 142–148. [CrossRef]

20. Dong, L.; Zhang, B.; Tang, C.; Li, B.; Zhou, L.; Gong, F.; Sun, B.; Gao, F.; Dong, L.; Chen, Y. Influence of CeO_2 Modification on the Properties of Fe_2O_3–$Ti_{0.5}Sn_{0.5}O_2$ Catalyst for NO Reduction by CO. *Catal. Sci. Technol.* **2014**, *4*, 482–493. [CrossRef]

21. Schmitt, R.; Nenning, A.; Kraynis, O.; Korobko, R.; Frenkel, A.I.; Lubomirsky, I.; Haile, S.M.; Rupp, J.L.M. A Review of Defect Structure and Chemistry in Ceria and Its Solid Solutions. *Chem. Soc. Rev.* **2020**, *49*, 554–592. [CrossRef]

22. Mastelaro, V.; Briois, V.; de Souza, D.P.; Silva, C.L. Structural Studies of a ZrO_2–CeO_2 Doped System. *J. Eur. Ceram. Soc.* **2003**, *23*, 273–282. [CrossRef]

23. Lambrou, P.S.; Savva, P.G.; Fierro, J.L.G.; Efstathiou, A.M. The Effect of Fe on the Catalytic Behavior of Model Pd-Rh/CeO_2-Al_2O_3 Three-Way Catalyst. *Appl. Catal. B Environ.* **2007**, *76*, 375–385. [CrossRef]

24. Vidmar, P.; Fornasiero, P.; Kašpar, J.; Gubitosa, G.; Graziani, M. Effects of Trivalent Dopants on the Redox Properties of $Ce_{0.6}Zr_{0.4}O_2$ Mixed Oxide. *J. Catal.* **1997**, *171*, 160–168. [CrossRef]

25. Jia, L.; Shen, M.; Wang, J.; Chu, X.; Wang, J.; Hu, Z. Redox Behaviors and Structural Characteristics of $Mn_{0.1}Ce_{0.9}O_x$ and $Mn_{0.1}Ce_{0.6}Zr_{0.3}O_x$. *J. Rare Earths* **2008**, *26*, 523–527. [CrossRef]

26. Zhang, L.; Spezzati, G.; Muravev, V.; Verheijen, M.A.; Zijlstra, B.; Filot, I.A.W.; Su, Y.-Q.; Chang, M.-W.; Hensen, E.J.M. Improved Pd/CeO_2 Catalysts for Low-Temperature NO Reduction: Activation of CeO_2 Lattice Oxygen by Fe Doping. *ACS Catal.* **2021**, *11*, 5614–5627. [CrossRef] [PubMed]

27. Martínez-Arias, A.; Fernández-García, M.; Gálvez, O.; Coronado, J.M.; Anderson, J.A.; Conesa, J.C.; Soria, J.; Munuera, G. Comparative Study on Redox Properties and Catalytic Behavior for CO Oxidation of CuO/CeO_2 and $CuO/ZrCeO_4$ Catalysts. *J. Catal.* **2000**, *195*, 207–216. [CrossRef]

28. Hornés, A.; Hungría, A.B.; Bera, P.; Cámara, A.L.; Fernández-García, M.; Martínez-Arias, A.; Barrio, L.; Estrella, M.; Zhou, G.; Fonseca, J.J.; et al. Inverse CeO_2/CuO Catalyst As an Alternative to Classical Direct Configurations for Preferential Oxidation of CO in Hydrogen-Rich Stream. *J. Am. Chem. Soc.* **2010**, *132*, 34–35. [CrossRef]

29. Perin, G.; Fabro, J.; Guiotto, M.; Xin, Q.; Natile, M.M.; Cool, P.; Canu, P.; Glisenti, A. $Cu@LaNiO3$ Based Nanocomposites in TWC Applications. *Appl. Catal. B Environ.* **2017**, *209*, 214–227. [CrossRef]

30. Dong, L.; Zhang, L.; Sun, C.; Yu, W.; Zhu, J.; Liu, L.; Liu, B.; Hu, Y.; Gao, F.; Dong, L.; et al. Study of the Properties of $CuO/VO_x/Ti_{0.5}Sn_{0.5}O_2$ Catalysts and Their Activities in NO + CO Reaction. *ACS Catal.* **2011**, *1*, 468–480. [CrossRef]

31. Koirala, R.; Pratsinis, S.E.; Baiker, A. Synthesis of Catalytic Materials in Flames: Opportunities and Challenges. *Chem. Soc. Rev.* **2016**, *45*, 3053–3068. [CrossRef] [PubMed]

32. Teoh, W.Y.; Amal, R.; Mädler, L. Flame Spray Pyrolysis: An Enabling Technology for Nanoparticles Design and Fabrication. *Nanoscale* **2010**, *2*, 1324–1347. [CrossRef] [PubMed]

33. Christensen, J.M.; Deiana, D.; Grunwaldt, J.-D.; Jensen, A.D. Ceria Prepared by Flame Spray Pyrolysis as an Efficient Catalyst for Oxidation of Diesel Soot. *Catal. Lett.* **2014**, *144*, 1661–1666. [CrossRef]

34. Michalow-Mauke, K.A.; Lu, Y.; Kowalski, K.; Graule, T.; Nachtegaal, M.; Kröcher, O.; Ferri, D. Flame-Made $WO_3/CeOx$-TiO_2 Catalysts for Selective Catalytic Reduction of NOx by NH_3. *ACS Catal.* **2015**, *5*, 5657–5672. [CrossRef]

35. Kydd, R.; Teoh, W.Y.; Wong, K.; Wang, Y.; Scott, J.; Zeng, Q.-H.; Yu, A.-B.; Zou, J.; Amal, R. Flame-Synthesized Ceria-Supported Copper Dimers for Preferential Oxidation of CO. *Adv. Funct. Mater.* **2009**, *19*, 369–377. [CrossRef]

36. Yang, F.; Liu, M.; Chen, X.; Xu, Z.; Zhao, H. Simultaneous Control over Lattice Doping and Nanocluster Modification of a Hybrid $CuOx/TiO_2$ Photocatalyst during Flame Synthesis for Enhancing Hydrogen Evolution. *Sol. RRL* **2018**, *2*, 1800215. [CrossRef]

37. Zhang, Z.; Yu, J.; Zhang, J.; Ge, Q.; Xu, H.; Dallmann, F.; Dittmeyer, R.; Sun, J. Tailored Metastable Ce–Zr Oxides with Highly Distorted Lattice Oxygen for Accelerating Redox Cycles. *Chem. Sci.* **2018**, *9*, 3386–3394. [CrossRef]

38. Lopes, D.; Zotin, F.; Palacio, L.A. Copper-Nickel Catalysts from Hydrotalcite Precursors: The Performance in NO Reduction by CO. *Appl. Catal. B Environ.* **2018**, *237*, 327–338. [CrossRef]

39. Liu, T.; Yao, Y.; Wei, L.; Shi, Z.; Han, L.; Yuan, H.; Li, B.; Dong, L.; Wang, F.; Sun, C. Preparation and Evaluation of Copper–Manganese Oxide as a High-Efficiency Catalyst for CO Oxidation and NO Reduction by CO. *J. Phys. Chem. C* **2017**, *121*, 12757–12770. [CrossRef]

40. Wang, Y.; Jiang, Q.; Xu, L.; Han, Z.-K.; Guo, S.; Li, G.; Baiker, A. Effect of the Configuration of Copper Oxide–Ceria Catalysts in NO Reduction With CO: Superior Performance of a Copper–Ceria Solid Solution. *ACS Appl. Mater. Interfaces* **2021**, *13*, 61078–61087. [CrossRef]

41. Chen, X.; Xu, Z.; Yang, F.; Zhao, H. Flame Spray Pyrolysis Synthesized CuO-TiO2 Nanoparticles for Catalytic Combustion of Lean CO. *Proc. Combust. Inst.* **2019**, *37*, 5499–5506. [CrossRef]

42. Meng, L.; Zhao, H. Low-Temperature Complete Removal of Toluene over Highly Active Nanoparticles CuO-TiO2 Synthesized via Flame Spray Pyrolysis. *Appl. Catal. B Environ.* **2020**, *264*, 118427. [CrossRef]

43. Xiong, Z.; Xu, Z.; Li, Y.; Dong, L.; Wang, J.; Zhao, J.; Chen, X.; Zhao, Y.; Zhao, H.; Zhang, J. Incorporating Highly Dispersed and Stable Cu^+ into TiO_2 Lattice for Enhanced Photocatalytic CO_2 Reduction with Water. *Appl. Surf. Sci.* **2020**, *507*, 145095. [CrossRef]

44. Jia, A.-P.; Hu, G.-S.; Meng, L.; Xie, Y.-L.; Lu, J.-Q.; Luo, M.-F. CO Oxidation over $CuO/Ce_{1−x}Cu_xO_{2−δ}$ and $Ce_{1−x}Cu_xO_{2−δ}$ Catalysts: Synergetic Effects and Kinetic Study. *J. Catal.* **2012**, *289*, 199–209. [CrossRef]

45. Gamarra, D.; Munuera, G.; Hungría, A.B.; Fernández-García, M.; Conesa, J.C.; Midgley, P.A.; Wang, X.Q.; Hanson, J.C.; Rodríguez, J.A.; Martínez-Arias, A. Structure−Activity Relationship in Nanostructured Copper−Ceria-Based Preferential CO Oxidation Catalysts. *J. Phys. Chem. C* **2007**, *111*, 11026–11038. [CrossRef]

46. Fornasiero, J.K.P.; Graziani, M. On the Rate Determining Step in the Reduction of CeO_2–ZrO_2 Mixed Oxides. *Appl. Catal. B Environ.* **1999**, *22*, L11–L14. [CrossRef]

47. Vidal, J.K.H.; Pijolat, M.; Colon, G.; Bernal, S.; Cordón, A.; Perrichon, V.; Fally, F. Redox Behavior of CeO_2–ZrO_2 Mixed Oxides. I. Influence of Redox Treatments on High Surface Area Catalysts. *Appl. Catal. B Environ.* **2000**, *27*, 49–63. [CrossRef]

48. Wang, S.-Y.; Li, N.; Luo, L.-F.; Huang, W.-X.; Pu, Z.-Y.; Wang, Y.-J.; Hu, G.-S.; Luo, M.-F.; Lu, J.-Q. Probing Different Effects of Surface MO_y and Mn^+ Species (M=Cu, Ni, Co, Fe) for $xMO_y/Ce_{y0.9}M_{0.1−x}O_{2−δ}$ Catalysts in CO Oxidation. *Appl. Catal. B Environ.* **2014**, *144*, 325–332. [CrossRef]

49. Granger, P.; Dujardin, C.; Paul, J.-F.; Leclercq, G. An Overview of Kinetic and Spectroscopic Investigations on Three-Way Catalysts: Mechanistic Aspects of the CO + NO and CO + N_2O Reactions. *J. Mol. Catal. A Chem.* **2005**, *228*, 241–253. [CrossRef]

50. Granger, P.; Dathy, C.; Lecomte, J.J.; Leclercq, L.; Prigent, M.; Mabilon, G.; Leclercq, G. Kinetics of the NO and CO Reaction over Platinum Catalysts-I. Influence of the Support. *J. Catal.* **1998**, *173*, 304–314. [CrossRef]

51. Wang, W.; Qu, Z.; Song, L.; Fu, Q. Probing into the Multifunctional Role of Copper Species and Reaction Pathway on Copper-Cerium-Zirconium Catalysts for CO_2 Hydrogenation to Methanol Using High Pressure in Situ DRIFTS. *J. Catal.* **2020**, *382*, 129–140. [CrossRef]

52. Christou, S.Y.; García-Rodríguez, S.; Fierro, J.L.G.; Efstathiou, A.M. Deactivation of $Pd/Ce_{0.5}Zr_{0.5}O_2$ Model Three-Way Catalyst by P, Ca and Zn Deposition. *Appl. Catal. B Environ.* **2012**, *111–112*, 233–245. [CrossRef]

53. Yang, S.; Zhu, W.; Jiang, Z.; Chen, Z.; Wang, J. The Surface Properties and the Activities in Catalytic Wet Air Oxidation over CeO_2–TiO_2 Catalysts. *Appl. Surf. Sci.* **2006**, *252*, 8499–8505. [CrossRef]

54. Chen, H.; Motuzas, J.; Martens, W.; da Costa, J.C.D. Degradation of Azo Dye Orange II under Dark Ambient Conditions by Calcium Strontium Copper Perovskite. *Appl. Catal. B Environ.* **2018**, *221*, 691–700. [CrossRef]

55. Sun, W.; Wei, H.; An, L.Y.; Jin, C.; Wu, H.; Xiong, Z.-A.; Pu, C.; Sun, C. Oxygen Vacancy Mediated La1-XCexFeO3-δ Perovskite Oxides as Efficient Catalysts for CWAO of Acrylic Acid by A-Site Ce Doping. *Appl. Catal. B Environ.* **2019**, *245*, 20–28. [CrossRef]

56. Moretti, E.; Lenarda, M.; Riello, P.; Storaro, L.; Talon, A.; Frattini, R.; Reyes-Carmona, A.; Jiménez-López, A.; Rodríguez-Castellón, E. Influence of Synthesis Parameters on the Performance of CeO_2–CuO and CeO_2–ZrO_2–CuO Systems in the Catalytic Oxidation of CO in Excess of Hydrogen. *Appl. Catal. B Environ.* **2013**, *129*, 556–565. [CrossRef]

57. Gholami, Z.; Luo, G. Low-Temperature Selective Catalytic Reduction of NO by CO in the Presence of O_2 over Cu:Ce Catalysts Supported by Multiwalled Carbon Nanotubes. *Ind. Eng. Chem. Res.* **2018**, *57*, 8871–8883. [CrossRef]

58. Mädler, L.; Kammler, H.; Mueller, R.; Pratsinis, S. Controlled Synthesis of Nanostructured Particles by Flame Spray Pyrolysis. *J. Aerosol Sci.* **2002**, *33*, 369–389. [CrossRef]

59. Mädler, L.; Stark, W.J.; Pratsinis, S.E. Flame-Made Ceria Nanoparticles. *J. Mater. Res.* **2002**, *17*, 1356–1362. [CrossRef]

60. Luo, M.-F.; Song, Y.-P.; Lu, J.-Q.; Wang, X.-Y.; Pu, Z.-Y. Identification of CuO Species in High Surface Area CuO−CeO_2 Cat-Alysts and Their Catalytic Activities for CO Oxidation. *J. Phys. Chem. C* **2007**, *111*, 12686–12692. [CrossRef]